WEP Warwick Evans Publishing

International Journal of Materials Science and Technology Studies

ISSN: 3006-7693 (Print), ISSN: 3006-3744 (Online) | Volume 4, Number 1, Year 2025
DOI: https://doi.org/10.62051/ijmsts.v4n1.05
Journal homepage: https://wepub.org/index.php/IJMSTS/index

Structural Characteristics and Anisotropic Carrier Mobility of Two-dimensional Carbon Nitride C12N2

Jian Liu *

College of Mathematical Sciences and Statistics, Baise University, Baise, China
*Corresponding Author: Jian Liu

ABSTRACT

Two-dimensional (2D) carbon nitrides are attracting growing interest because of their structural diversities and distinctive electronic properties. A first principles investigation has been carried out on a new 2D carbon nitride $C_{12}N_2$ with orthorhombic lattice. The carbon nitride $C_{12}N_2$ shows medium electronic band gap of 1.01 eV, high carrier mobility about of 2.2×10^5 $cm^2V^{-1}s^{-1}$, suggesting that it is a promising candidate used on short channel transistors. The strain behavior of $C_{12}N_2$ has been studied, revealing that it can endure a uni-axial strain or compression of up to ±10%. Furthermore, the band edge positions, effective masses and band gap are seriously changed under different level of strains. It suggests that appropriate tensile strain can effectively overcome the short channel effect in semiconductor device.

KEYWORDS

First principles; Carbon nitrides; Structural Characteristics; Carrier Mobility

1. INTRODUCTION

Two-dimensional (2D) semiconductors hold great significance because of their potential applications in the next generation electronic devices, the research on 2D carbon materials has advanced rapidly and vigorously [1-4]. As the most stable 2D carbon material, Graphene has Dirac fermions act as massless carriers resulting in a high carrier mobility [5, 6]. However, due to its zero band gap, it is difficult to be applied in electronic devices. Graphdiyne (GDY), another kind of 2D carbon materials, composed of sp hybridized carbon atoms with various electronic properties spanning from semimetals to semiconductors [7]. In 2015, nitrogenated holey graphene (NHG) was synthesized through a wet chemical reaction [8]. The monolayer NHG has a C_2N stoichiometry with evenly spaced periodic holes in a fused aromatic network structure and it is behaving semiconductor characteristics with a band gap of 1.96 eV. Another type of graphitic carbon nitride with CN stoichiometry was also synthesized [9]. This monolayer graphitic carbon nitride is discovered to be a semiconductor having a band gap of 2.89 eV, and as the quantity of layers goes up, the band gap reduces. The properties of 2D materials, including mechanical, electronic, and thermalelectric ones, can be notably adjusted by incorporating foreign atoms into their structures. As carbon's neighboring element in the periodic table, the nitrogen atom has been extensively used to dope in 2D carbon materials [10- 12], leading to a series of 2D carbon nitride materials. In recent experiments, some of these have been synthesized, like C_3N_4 [13], C_2N [14], and C_3N [15]. Unlike graphene, these 2D carbon nitrides are semiconductors having band gaps that range from 1.96 eV to 2.70 eV, but their carrier mobilities are frequently rather low.

In this work, a new 2D carbon nitride material, with hybridized carbon atoms like in graphyne and pyridine nitrogen atoms, has been investigated. The graphyne-like carbon nitride $C_{12}N_2$ have

Content from this work may be used under the terms of CC BY-NC 4.0 licence (https://creativecommons.org/licenses/by-nc/4.0/).
Published by Warwick Evans Publishing.

orthorhombic lattice with different lengths of acetylene bonds. A direct band gap of 1.01eV was predicted based on the lattice structure and length of acetylene bonds. High carrier mobility on the order of 2.2×10^5 $cm^2V^{-1}s^{-1}$, high flexibility with critical strain up to 10%, and band alignment were also demonstrated through first principles calculations. The band gaps can also be effectively tuned by applying external strain.

2. METHOD AND COMPUTATIONAL DETAILS

Within the density functional theory framework, as implemented in the Vienna ab initio simulation package (VASP) [16], structural optimization and property calculations are carried out. The ion - electron interaction is realized by the projector - augmented plane wave (PAW) approach. The electronic exchange correlation functional is dealt with using the generalized gradient approximation (GGA) in the form put forward by Perdew, Burke and Ernzerhof (PBE) [17]. The energy cutoff of the plane waves is set at 700 eV, with an energy precision of 10^{-6} eV. Atomic positions are fully relaxed until the force on each atom is below 10^{-3} eV/Å. To simulate the monolayer, the supercell method is employed, where a vacuum distance of about 20 Å is used to remove the interaction between adjacent layers. Given that the GGA generally underestimates the band gaps, we use the Heyd−Scuseria−Ernzerhof (HSE06) [18] hybrid functional to compute the band structures and optical absorption coefficients. Dynamic stabilities and phonon dispersion curves are calculated with the supercell approach as implemented in the Phonopy code [19]. The integration of the Brillouin zone was sampled using a k-point mesh of 11×11×1. The mechanical properties were computed from the strain energy corresponding to the in-plane lattice distortion.

3. RESULTS AND DISCUSSION

3.1. The Structural Geometry of $C_{12}N_2$

As shown in Figure 1, it is found that a new $C_{12}N_2$ monolayer stabilizes into a trigonal structure. The basic building unit is a $C_{24}N_4$ unit, where a C_4N_2 ring lies at the center, surrounded by four other end - sharing C_4 chains, similar to the arrangement of benzene. Interestingly, an alternating arrangement of ethylene - like C_2 units connected by two N atoms forms the outer edge ring of the $C_{18}N_6$ unit.

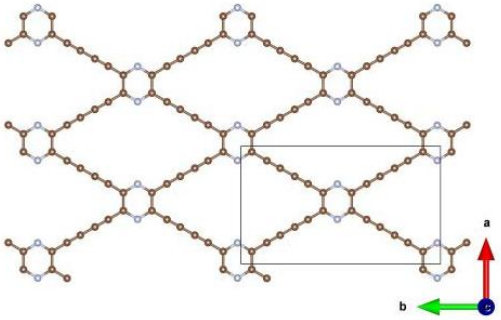

Figure 1. The structural geometry of $C_{12}N_2$. Nitrogen and carbon atoms are represented by gray and brown balls, respectively. The rhombuses indicate the primitive cells of these lattices

On the other hand, each N atom is linked to two C atoms, forming a C_2N unit, having the same geometric configuration as in C_3N. The optimized lattice constants of $C_{12}N_2$ is a=9.46 Å, b=16.09 Å. The C - C bond length in the C_4N_2 rings is 1.44 Å, nearly the same as the sp2 C - C bond length in graphene (1.42 Å). The N - C bond length in the C_4N_2 rings is of 1.34Å is also similar to 1.36 Å in another carbon nitride C_3N monolayer. The C-C bond length in the C_4 chains is 1.23 Å, these values are slightly longer than those of $C(sp^2)$-C(sp) bonds 1.40Å in graphyne (graphdiyne), C(sp)-C(sp) bonds 1.33 Å, and $C(sp^2)=C(sp^2)$ bonds 1.42 Å (1.41 Å) in graphyne (graphdiyne). The lengths of the $C(sp^2)=N(sp^2)$ bonds are 1.34 Å, very close to that in C_2N (1.34 Å). The analysis of the electron

localization function clearly reveals that the bonds between nearest - neighbor C atoms or between N and C atoms are covalent. Notably, there is a non - bonding lone electron pair around each N atom .

Overall, the unique atomic arrangement, the bond characteristics and the existence of electron pair in C_4N_2 suggest that C atoms are in the sp^2 configuration and N atoms undergo sp^3 hybridization, where one of the hybrid orbitals is occupied by alone electron pair, and the other three hybrid orbitals form covalent bonds with neighboring C atoms. Actually, these bonding configurations meet the chemical octet rule on both C and N sites, inevitably enhancing its structural stability. On the other hand, the arrangement of N and C atoms in zigzag and armchair directions is clearly different.

3.2. The Electronic Band Structures of $C_{12}N_2$

Compared with graphene, $C_{12}N_2$ exhibits distinct structural properties and chemical bonds that could lead to unanticipated physical properties. The $C_{12}N_2$ monolayer is a direct gap semiconductor with a 1.01 eV band gap at the Γ point (Figure 2), calculated using the HSE06 hybrid functional. To further investigate the source of its semiconducting nature, we computed the band decomposed charge density. The charge density of the valence band maximum (VBM) is distributed on the outer edge ring of the basic building block. Nevertheless, the charge density of N atoms, existing as lone electron pairs, separates the π electrons from the C 2pz orbitals of ethylene-like C_2 units. Thus, the existence of lone electron pairs in N atoms and their unique arrangement impede the formation of extended π electron states. To verify this, we constructed a hypothetical $C_{12}N_2$ where all atoms are arranged in a plane, disrupting the sp^3 hybridization of N. As anticipated, this hypothetical $C_{12}N_2$ structure is metallic. On the contrary, the charge density related to the conduction band minimum (CBM) is distributed across the entire monolayer. Once again, the lone electron pair of N atoms is not linked to the charge densities of other atoms.

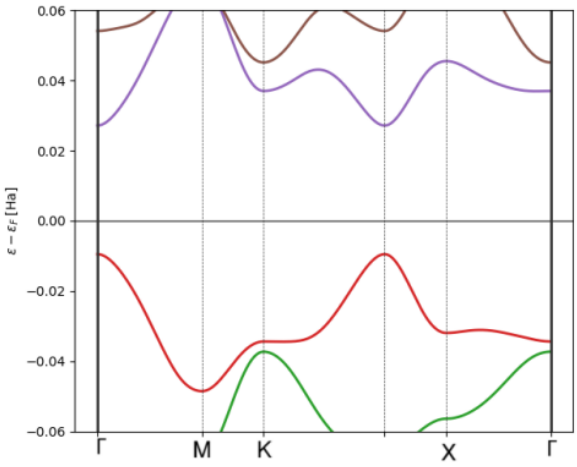

Figure 2. The electronic band structures of $C_{12}N_2$, which are calculated by HSE06 functional. Special points in Brillouin zone are set as M (0 0.5 0), X (0.5 0 0), Γ (0 0 0) and K (-0.33 0.67 0)

The band lines with dispersion in the vicinity of the Fermi level of the kagome and rhombic lattices suggest the high carrier mobility of these 2D carbon nitride materials. To verify this conjecture, we computed the carrier mobility based on an acoustic phonon limited scattering model. According to the model, the carrier mobility can be expressed. m^*_d is the average effective mass determined by $m^*_d = (m^*_x m^*_y)^{1/2}$, m^*_e is the effective mass, E_i is the deformation potential defined as $E_i = \Delta V_i/(\Delta l/l_0)$, ΔV_i is the variation in the band energy, l_0 is the lattice constant in the zigzag or armchair direction, Δl is the deformation of l_0. The in-plane stiffness constant is acquired by evaluating the strain energy curve. All the computations were carried out at the GGA - PBE level. We can observe the following characteristics. (1) Electrons possess higher mobility than holes by over one order, because of the larger deformation potential of VBM, which characterizes the coupling strength of holes with the acoustic phonons. (2) Lattices have higher carrier mobility owing to the larger in-plane stiffness and

smaller effective masses. (3) As the length of acetylenic linkages increases, lattices display different behaviors in carrier mobility. The carrier mobility of the kagome lattice declines with the increase of acetylenic linkages, while an opposite trend is found for the rhombic lattice. (4) The carrier mobility of the rhombic lattice shows significant anisotropy.

Table 1. The carrier mobility in $C_{12}N_2$. e and h denote the electrons and holes. m_e^* is the carrier effective mass along the zigzag and the armchair directions

		m^*_e/m_0	m^*_e/m_0	E_{1zz}	E_{1am}	C_{zz}	C_{am}	μ_{zz}	μ_{am}
		zigzag	armchair	(eV)		(J/m^2)		($10^3 cm^2V^{-1}s^{-1}$)	
$C_{12}N_2$	e	0.21	0.09	1.21	1.32	211.1	29.3	163.61	54.75
	h	0.13	0.09	6.76	2.95	211.1	29.3	10.42	12.87

The effective masses for holes are 0.13 m_0 (0.09 m_0) and for electrons are 0.21 m_0 (0.09 m_0) along the zigzag (armchair) direction. These values are much smaller than the effective mass values of monolayer and few-layer black phosphorene, and larger than that in graphene. Intriguingly, the effective masses of $C_{12}N_2$ are highly isotropic, which matches the nearly symmetric energy band structure. Additionally, the in-plane stiffness values are isotropic too, and significantly larger than those in phosphorene and MoS_2. On the contrary, the direction dependent anisotropy can be grasped by the distinct arrangement of N and C atoms along zigzag and armchair directions. The calculated electron mobility along the armchair direction is 2.2×10^5 $cm^2V^{-1}s^{-1}$, which is an order of magnitude greater than the hole mobility (2.4×10^4 $cm^2V^{-1}s^{-1}$). That is to say, electron transport is promoted along the armchair direction, while the zigzag direction is conducive to hole transport. Since the stiffness and effective mass are isotropic, the direction - dependent deformation potentials are mainly accountable for the anisotropic charge transport. Notably, both hole and electron mobility are much higher than that in phosphorene (~10^4 $cm^2V^{-1}s^{-1}$) and comparable to graphene (3.2~3.5×10^5 $cm^2V^{-1}s^{-1}$). Based on the above analysis, the high carrier mobility of $C_{12}N_2$ can be ascribed to the large in plane stiffness, the small effective mass, and small deformation potential. Moreover, we also investigate the influence of the biaxial strain on the electronic properties of $C_{12}N_2$. Curiously, its direct band gap characteristic still persists within compressive or tensile 5%. Nevertheless, the band gap gets larger under compression, and the opposite occurs when it is stretched. More curiously, under compression, $C_{12}N_2$ exhibits a strong hole transport ability, while it favors electron transport when stretched, suggesting that conductivity can be effectively regulated with strain.

3.3. The Stress-Strain Responses of $C_{12}N_2$

The crucial strains of these graphyne-like carbon nitrides were ascertained by applying uniaxial and biaxial strains along the zigzag and armchair directions. The applied strain ε is defined as $\varepsilon=(a - a_0)/a_0$, where a and a_0 are the lattice constants of strained and unstrained materials respectively. The stress is acquired by differentiating the energy density $dE/d\varepsilon$ with respect to strain. Notably, the critical strain evaluated using this approach cannot be directly compared to the experimental data, since uniaxial loading rather than uniaxial strain is applied in experiments. Additionally, the supercell ought to be large enough to capture crack propagation, dislocation generation and other effects occurring in realistic materials to obtain a reliable result. Anyway, the critical strains evaluated using the current strategy can be regarded as the upper limits of these 2D carbon nitrides and can be compared with those of other 2D materials obtained using the same approach.

We additionally explore the stress-strain responses of monolayer $C_{12}N_2$ sheet along the zigzag or armchair directions. This study is carried out via first principles calculations based on DFT. The outcome indicates that the tensile strength of monolayer $C_{12}N_2$ is 31.7 GPa.nm along the armchair direction and 29.5 GPa.nm along the zigzag direction. From our results, it is not discovered that $C_{12}N_2$ shows an evident anisotropy. Previously, Mortazavi et al. also examined the tensile strength of monolayer C_3N. The tensile strength is 35.2 GPa.nm along the armchair direction and 32.8 GPa.nm

along the zigzag direction, which implies that the C_3N sheet displays anisotropy. The results also reveal that the C - N bonds are entirely broken at 12% along the armchair direction and at 11% along the zigzag direction. It is noted that more electrons are located at the cracking position, which suggests that the C - N bond is stable and can retain good strength.

3.4. The Thermoelectric Properties of $C_{12}N_2$

The electrical conductivities of the $C_{12}N_2$ sheet in different crystallographic directions exhibit the same temperature dependent trend (Fig. 3). We notice three regions: initially, metallic transport behavior from 300 to 500 K; next, a shift to thermally activated semiconducting behavior up to about 800 K; and beyond that, a nearly temperature independent trend up to 900 K. The first increase above 500 K is ascribed to the thermal excitation of carriers, while the second is associated with the phase transition from Pnma to the Cmcm space group. It is easy to observe that the electrical conductivities along the armchair direction is lower along the zigzag direction. This anisotropy results from the higher ratio of Hall coefficient to resistivity within the plane of the $C_{12}N_2$ slabs than perpendicular to them. The Seebeck coefficients display almost isotropic behavior and are independent of crystallographic directions (Fig. 3). The gradual decline of the Seebeck coefficients above 500 K is in line with the increasing trend in the electrical conductivity and implies bipolar conduction and an increasing inverse Hall coefficient. This behavior agrees with our electronic band structure calculations, which indicate that the band gap decreases significantly from Pnma to Cmcm, and thus a bipolar conduction process is anticipated as the temperature rises.

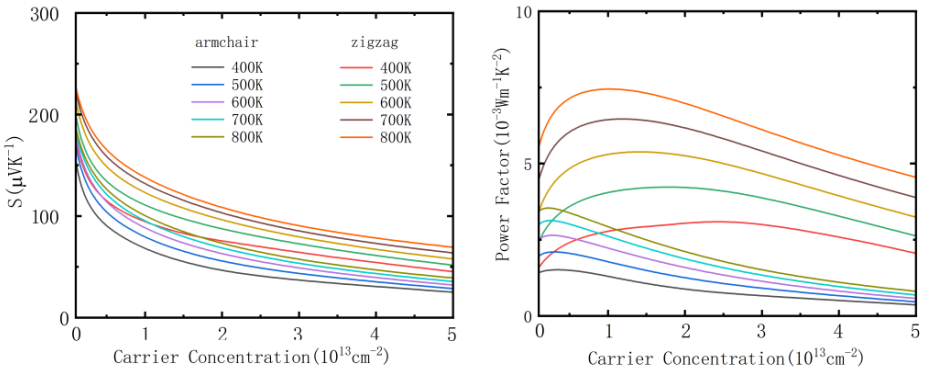

Figure 3. Thermoelectric properties as a function of carrier concentration for $C_{12}N_2$ sheet: Seebeck coefficient and Power factor, PF

Compared to the other two axial directions around 800 K (Fig. 3), the power factor along the zigzag direction exhibits the highest value (7.6 $mWcm^{-1}K^{-2}$); the maximum power factor at 800 K along the armchair direction is 3.6 $mWcm^{-1}K^{-2}$. When compared with other state-of-the-art thermoelectrics, the power factors achieved in the $C_{12}N_2$ sheet are moderate, yet they are significantly higher than those in other thermoelectrics with inherently low overall thermal conductivity (e.g., $Yb_{14}MnSb_{11}$, Ag_6TlTe_5, $AgSbTe_2$). The highest power factor along the zigzag direction is twice as high as that along the armchair direction.

4. SUMMARY

We propose a novel two dimensional carbon nitride made up of sp and sp^2 hybridized carbon atoms and nitrogen atoms. A first principles study has been conducted on a new 2D carbon nitride $C_{12}N_2$ with an orthorhombic lattice. The carbon nitride $C_{12}N_2$ exhibits a medium electronic band gap of 1.01 eV and high carrier mobility of around 2.2×10^5 $cm^2V^{-1}s^{-1}$, indicating that it is a promising option for use in short channel transistors. The strain behavior of $C_{12}N_2$ has been explored, showing that it can withstand a uniaxial strain or compression of up to ±10%. The band gap of $C_{12}N_2$ can be increased to 1.50 eV under the bi-axial strain. In order to overcome short channel effect, the high permittivity

materials (high-k) and 2D semiconductor have to be introduced into MOSFETs. The conduction band offset rises with the strain, which implies that appropriate tensile strain can effectively overcome the short channel effect in semiconductor devices.

REFERENCES

[1] Xu M., Liang T., Shi M., et al. Graphene-like two-dimensional materials [J]. Chemical Reviews, 2013, 113(5): 3766-3798. https://doi.org/10.1021/cr300263a

[2] Li Y., Xu L., Liu H., et al. Graphdiyne and graphyne: from theoretical predictions to practical construction [J]. Chemical Society Reviews, 2014, 43(8):2572-2586. https://doi.org/10.1039/c3cs60388a

[3] Chen M., Han X., Tang K.. Topological regulations of Stone-Wales graphene [J]. Carbon, 2024, 226(000):15. https://doi.org/10.1016/j.carbon.2024.119163

[4] Wang Hai-Rui, Hou En-Hui, Xu N., et al. Photoelectrochemical Solution Gated Graphene Field-Effect Transistor Functionalized by Enzymatic Cascade Reaction for Organophosphate Detection [J]. Small, 2024, 20(44). https://doi.org/10.1002/smll.202402655

[5] Novoselov K. S., Geim A. K., Morozov S. V., et al. Two-Dimensional Gas of Massless Dirac Fermions in Graphene [J]. Nature, 2005. https://doi.org/10.1038/nature04233

[6] Zhang H., Xia Y., Bu H., et al. Graphdiyne: A promising anode material for lithium ion batteries with high capacity and rate capability [J]. Journal of Applied Physics, 2013, 113(4):183103. https://doi.org/10.1063/1.4789635

[7] Xu Z., Lv X., Li J., et al. A promising anode material for sodium-ion battery with high capacity and high diffusion ability: graphyne and graphdiyne [J]. RSC Advances, 2016, 6. https://doi.org/10.1039/C6RA01870J

[8] Mortazavi B., Rahaman O., Rabczuk T., et al. Thermal conductivity and mechanical properties of nitrogenated holey graphene [J]. Carbon, 2016, 106:1-8. https://doi.org/10.1016/j.carbon.2016.05.009

[9] Niu P., Yin L. C., Yang Y. Q., et al. Increasing the Visible Light Absorption of Graphitic Carbon Nitride (Melon) Photocatalysts by Homogeneous Self-Modification with Nitrogen Vacancies [J]. Advanced Materials, 2015, 26(47):8046-8052. https://doi.org/10.1002/adma.201404057

[10] Tian J., Liu Q., Ge C., et al. Ultrathin graphitic carbon nitride nanosheets: a low-cost, green, and highly efficient electrocatalyst toward the reduction of hydrogen peroxide and its glucose biosensing application [J]. Nanoscale, 2013, 5(19):8921-8924. https://doi.org/10.1039/c3nr02031b

[11] Ran J., Ma T. Y., Gao G., et al. Porous P-doped graphitic carbon nitride nanosheets for synergistically enhanced visible-light photocatalytic H_2 production [J]. Energy & Environmental Science, 2015, 8(12):3708-3717. https://doi.org/10.1039/C5EE02650D

[12] Wu M., Wang Q., Sun Q., et al. Functionalized Graphitic Carbon Nitride for Efficient Energy Storage [J]. The Journal of Physical Chemistry C, 2013, 117(12):6055–6059. https://doi.org/10.1021/jp311972f

[13] Yu Lijuan, Zhang Xiaohu, Zhuang Chuansheng, et al. Syntheses of asymmetric zinc phthalocyanines as sensitizer of Pt-loaded graphitic carbon nitride for efficient visible/near-IR-light-driven H_2 production [J]. Physical Chemistry Chemical Physics, 2014, 16(9):4106-4114. https://doi.org/10.1039/c3cp54316a

[14] Shinde S. S., Sami A., Lee J. H. Electrocatalytic hydrogen evolution using graphitic carbon nitride coupled with nanoporous graphene co-doped by S and Se [J]. Journal of Materials Chemistry A, 2015, 3(24):12810-12819. https://doi.org/10.1039/c5ta02656c

[15] Sui Y., Liu J., Zhang Y., et al. Dispersed conductive polymer nanoparticles on graphitic carbon nitride for enhanced solar-driven hydrogen evolution from pure water [J]. Nanoscale, 2013, 5(19):9150-9155. https://doi.org/10.1039/c3nr02413j

[16] Jürgen Hafner. Ab-initio simulations of materials using VASP: Density-functional theory and beyond [J]. Journal of Computational Chemistry, 2008, 29(13):2044-2078. https://doi.org/10.1002/jcc.21057

[17] Perdew J. P., Burke K., Ernzerhof M. Generalized Gradient Approximation Made Simple [J]. Physical Review Letters, 1998, 77(18):3865-3868. https://doi.org/10.1103/PhysRevLett.77.3865

[18] Deak P., Aradi B., Frauenheim T., et al. Accurate defect levels obtained from the HSE06 range-separated hybrid functional [J]. Physical review. B, Condensed matter, 2010, 81 (15): 2149-2149. https://doi.org/10.1103/PhysRevB.81.153203

[19] Togo A. First-principles Phonon Calculations with Phonopy and Phono3py [J]. Journal of the Physical Society of Japan, 2023. https://doi.org/10.7566/jpsj.92.012001